# We are IntechOpen, the world's leading publisher of Open Access books Built by scientists, for scientists

**4,800**
Open access books available

**122,000**
International authors and editors

**135M**
Downloads

Our authors are among the

**154**
Countries delivered to

**TOP 1%**
most cited scientists

**12.2%**
Contributors from top 500 universities

CLARIVATE ANALYTICS BOOK CITATION INDEX INDEXED

WEB OF SCIENCE™

Selection of our books indexed in the Book Citation Index in Web of Science™ Core Collection (BKCI)

## Interested in publishing with us?
## Contact book.department@intechopen.com

Numbers displayed above are based on latest data collected.
For more information visit www.intechopen.com

# 2

# Iron and Manganese-Containing Flavonol 2,4-Dioxygenase Mimics

József Kaizer, József Sándor Pap and Gábor Speier
*Department of Chemistry, University of Pannonia, Veszprém*
*Hungary*

## 1. Introduction

Oxygenases are enzymes which play key roles in the metabolism of essential substances for vital functions, and in the biodegradation of aromatic compounds in the environment. Two types of oxygenases are known, namely mono- and dioxygenases: one atom oxygen is incorporated into a substrate by the former accompanied with the formation of water, and two atoms of dioxygen into one or two substrates by the latter (Eqs. 1-3).

$$S + O_2 + e^- + H^+ = SO + H_2O \quad (1)$$

$$S + O_2 = SO_2 \quad (2)$$

$$S + S' + O_2 = SO + S'O \quad (3)$$

The oxygenases are metal-containing proteins and a fair number of them utilizes copper, manganese or iron at their active sites (Bugg, 2001). The dioxygenases as a subclass of these enzymes degrade cyclic organic substrates such as catechols and flavonoids. Catechol dioxygenases that act on ortho-dihydroxylated aromatic compounds are divided into two classes, namely intradiol and extradiol, which differ in their mode of ring cleavage and the oxidative state of the active-site metal (Kovaleva & Lipscomb, 2007). Intradiol enzymes contain an iron(III) center that is ligated by two histidines (His) and 2 tyrosines (Tyr) residues, while extradiol enzymes utilize iron(II) or, rarely manganese(II), that is coordinated by 2 histidines and 1 glutamic acid (Glu) residues. A fundamental question in the study of the catechol dioxygenases is: what factors control the choice of intradiol vs. extradiol specificity? The catalytic mechanism of intradiol cleavage has been proposed via activation of the catechol substrate by iron(III) to give an iron(II) semiquinone, which reacts directly with dioxygen to give a hydroperoxide intermediate, which then undergoes Criegee rearrangement via acyl migration to give muconic anhydride, as shown in Figure 1a. The catalytic mechanism of extradiol cleavage has been proposed also to involve one-electron transfer to give an iron(II)-superoxide-semiquinone complex, which recombines to form a hydroperoxide intermediate, which undergoes Criegee rearrangement via alkenyl migration to give an α-keto lactone intermediate, as shown in Figure 1b (Bugg & Ramaswamy, 2008). These compounds are important dietary components and have attracted considerable attention owing to their antioxidizing properties. Flavonoids are polyphenolic compounds that are widely distributed in vascular plants, and form active constituents of a number of herbal and traditional medicines.

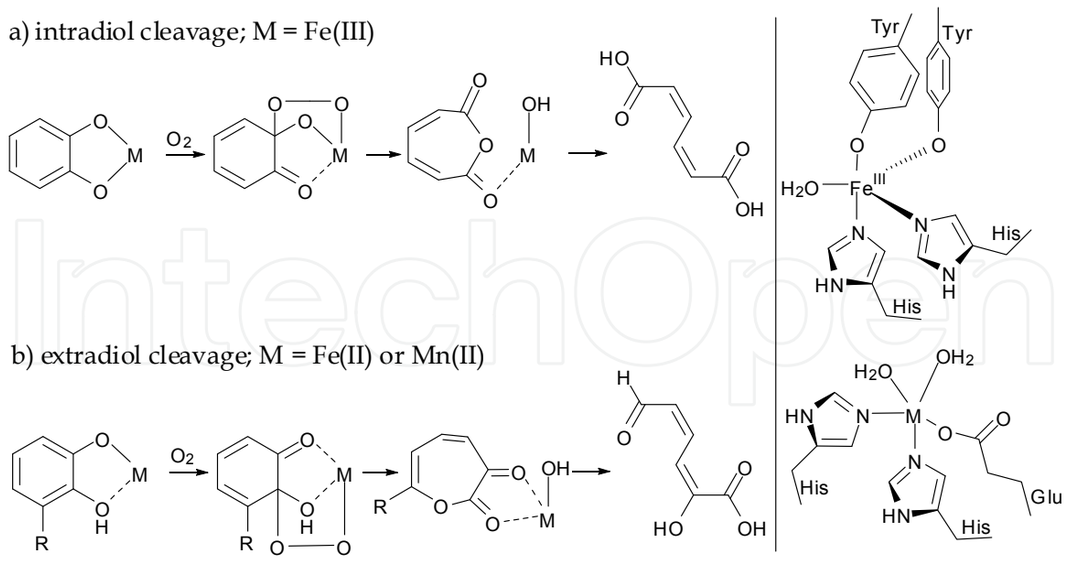


Fig. 1. Two modes of catechol cleavage catalyzed by intradiol and extradiol catechol dioxygenases.

In the soil environment, fungal and bacterial flavonol 2,4-dioxygenases (quercetinases) catalyze the oxidative degradation of flavonols to a depside (phenolic carboxylic acid esters) with concomitant evolution of carbon monoxide. Flavonol 2,4-dioxygenase was first recognized more than four decades ago in species of *Aspergillus* grown on rutin, and quercetinases from *Aspergillus flavus* (Oka et al., 1972), *Aspergillus niger* (Hund et al., 1999), and *Aspergillus japonicus* have been isolated (Kooter et al., 2002), purified, characterized, and the crystal structure of the title enzyme from *Aspergillus japonicus* has been reported (Fusetti et al., 2002). The diffraction studies showed that the enzyme forms homodimers, and each unit is mononuclear, with a type 2 copper center. Interestingly, an X-ray structure of *Aspergillus japonicus* anaerobically complexed with the natural substrate quercetin indicated that flavonols bind to the copper ion in a monodentate fashion. With the availability of the sequence and structural parameters for *Aspergillus japonicus* flavonol 2,4-dioxygenase, homologous enzymes were sought from other species. A BLAST search conducted against the sequence of *Aspergillus japonicus* identified the YxaG protein from *Bacillus subtilis* (Bowater et al., 2004), as the protein with the highest degree of similarity. Both enzymes belong to the cupin superfamily, in which the cupin domain compraises two conserved motifs. These two motifs have been found to ligate a number of divalent metal ions (e.g., Mn(II), Cu(II), and Fe(II)), which are ligated by two histidines and glutamic acid from motif 1 and a histidine residue from motif 2 (Schaab et al., 2006). Recent studies have been described the protein *YxaG* as an iron-containing flavonol 2,4-dioxygenase, but direct evidence for the natural cofactor is still missing (Gopal et al., 2005). Metal-substituted flavonol 2,4-dioxygenases were generated by expressing the enzyme in *Escherichia coli* grown on minimal media in the presence of various divalent metals. It was found that the addition of Mn(II), Co(II), and Cu(II) generated active enzymes, but the addition of Zn(II), Fe(II), and Cd(II) didn't increase the flavonol 2,4-dioxygenase activity (Schaab et al., 2006). The turnover number of the Mn(II)-containing enzyme was found to be in the order of 25 $s^{-1}$, nearly 40-fold higher than that of the Fe(II)-containing enzyme and similar in magnitude to

that of the Cu(II)-containing flavonol 2,4-dioxygenase from *Aspergillus japonicus*. On the basis of earlier kinetic and spectroscopic data it can be said that Mn(II) might be the preferred cofactor for this enzyme and that the catalytic enzyme mechanism is different from that of the *Aspergillus* species. After formation of the flavonoxyl-manganese-superoxide intermediate, the reaction could proceed via two pathways (Fig. 2, a and b). In the first pathway (a), the superoxide intermediate reacts with the flavonoxyl radical to form a lactone intermediate and a hydroxide ion via a Criegee intermediate. A Baeyer-Villiger rearrangement with alkyl migration would then generate the final products. This is identical to the mechanism proposed for extradiol catechol dioxygenases. In the second pathway (b), a 2,4-endoperoxide intermediate is formed and decomposes into the depside and carbon monoxide, similar to the mechanism proposed for the *Aspergillus* flavonol 2,4-dioxygenase.

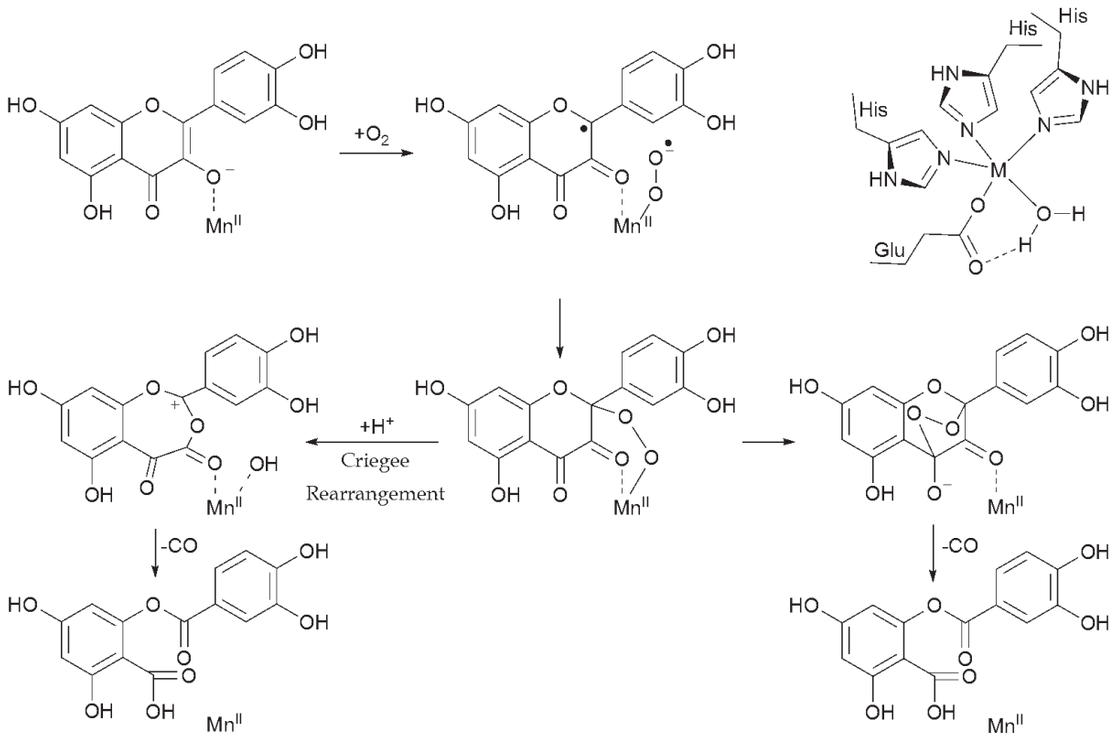


Fig. 2. Proposed mechanism of flavonol 2,4-dioxygenase from *B. subtilis* (Schaab et al., 2006).

Interestingly, recent investigations of flavonol 2,4-dioxygenase from *Streptomyces sp*. FLA expressed in *E. coli* revealed that this enzyme is most active in the presence of Ni(II), with the next highest level of activity being found with Co(II). In this case the nonredox role of the metal center was proposed (Merkens et al., 2008).

Studies on structural and functional models are important in order to elucidate the mechanism of the enzyme reaction. Extensive studies report on the coordination chemistry of flavonols with various metal ions. Recent crystallographic studies of flavonolato complexes of copper(I), copper(II), cobalt(III), and zinc(II) disclosed the coordination mode of the flavonolate ligand, geometries around the metal ions, and their influence on the delocalization of π-electrons in the flavonolate ligand, but only few examples are known for iron and manganese-containing systems. The stability of the metal flavonolates above can be

explained by the chelation and formation of a stable five-membered ring in the flavonolate complexes. It can be assumed that the coordination mode of the substrate in the enzymatic and model systems could give rise to differences in the degradation rates. Apart from the coordination mode of flavonolate ligands, it is important to know how the flavonolate ligand is activated for the reaction with molecular oxygen. From our earlier results obtained both with redox and non-redox metal-containing systems, the conclusion could be drawn that the oxygenolysis of the flavonolate ion in aprotic solvents takes place via an 2,4-endoperoxide intermediate (Kaizer et al., 2006; Pap et al., 2010).

Since there is no manganese- or iron-containing systems in the literature, in this book we report details for synthesis and characterization of some manganese and iron(III) flavonolate complexes as synthetic models for the *YxaG* dioxygenase, and their direct and carboxylate-enhanced dioxygenation compared to the copper-containing models, respectively. We will show that bulky carboxylates as coligands dramatically enhance the reaction rate, which can be explained by two different mechanisms, caused by the formation of more reactive monodentate flavonolate complexes.

## 2. Model systems

### 2.1 Synthetic enzyme-substrate (ES) models

Synthetic manganese and iron complexes have been synthesized and characterized by IR, UV-vis spectroscopy and X-ray crystallography (Fig. 3) (Baráth et al., 2009; Kaizer et al., 2007). Compounds $Mn(fla)_2(py)_2$ (flaH = flavonol) $Fe(4'MeOfla)_3$ and Fe (4'Rfla)(salen) ($salenH_2$ = 1,6-bisz(2-hydroxyphenyl)-2,5-diaza-hexa-1,5-diene, R = H, MeO, Cl, $NMe_2$) have very similar IR and electronic spectra. Coordination of the substrate flavonol to the manganese and iron sites is indicated by the characteristic $\nu_{CO}$ band between 1540 and 1580 $cm^{-1}$ (Table 1). Compared to that of the $\nu_{CO}$ vibration at 1602 $cm^{-1}$ of free flavonol this band is shifted by 30-70 $cm^{-1}$ to lower energies. This can be interpreted by the formation of a stable five-membered chelate that is formed upon the coordination of the 3-OH and 4-CO oxygen atoms of flavonol. The highest energy $\nu_{CO}$ is found for the complex Fe(fla)(salen), which is consistent with the structural data for Fe(fla)(salen). With increasing the difference in M-O distances ($\Delta_{M-O}$) in the chelate the $\nu_{CO}$ value shows an increase. The $Mn(fla)_2(py)_2$ complex exhibits the lowest energy $\nu_{CO}$ vibration.

In the UV-vis absorption spectrum the bathochromic shift of the flavonol π-π* transition, which is termed band I from ~340 nm, and the hypsochromic shift of the absorption band is found relative to the free flavonolate anion from 465 nm (Barhács et al., 2000) to 400-440 nm shows unambiguously the presence of the coordinated substrate. For example $Mn(fla)_2(py)_2$, exhibits band I at 433 nm. This matches well with the band I reported for [6-$Ph_2$TPA)Mn(fla)]OTf (6-$Ph_2$TPA = *N*,*N*-bis((6-phenyl-2-pyridil)methyl)-*N*-((2-pyridyl)-methyl)amine) (431 nm) (Grubel et al., 2010). The hypsochromic shift of the absorption band I (π-π*) of the coordinated flavonolate ligand increases in the order Cu(II) ~ Mn(II) < Fe(III). In case of the $Fe(4'MeOfla)_3$ a shoulder at 680 nm and a maximum at 530 nm are characteristic of an octahedral arrangement around the ferric ion, that are assigned to the $^6A_{1g} \rightarrow {}^4T_{1g}$ and $^6A_{1g} \rightarrow {}^4T_{2g}$ transitions, respectively.

The molecular structure and atom numbering scheme for complex $Mn(fla)_2(py)_2$ can be seen in Fig. 4. The manganese has a slightly distorted tetragonal bipyramidal geometry, which possesses high symmetry with trans coordination of the flavonolate ligands in the basal plane and the two pyridines in apical positions.

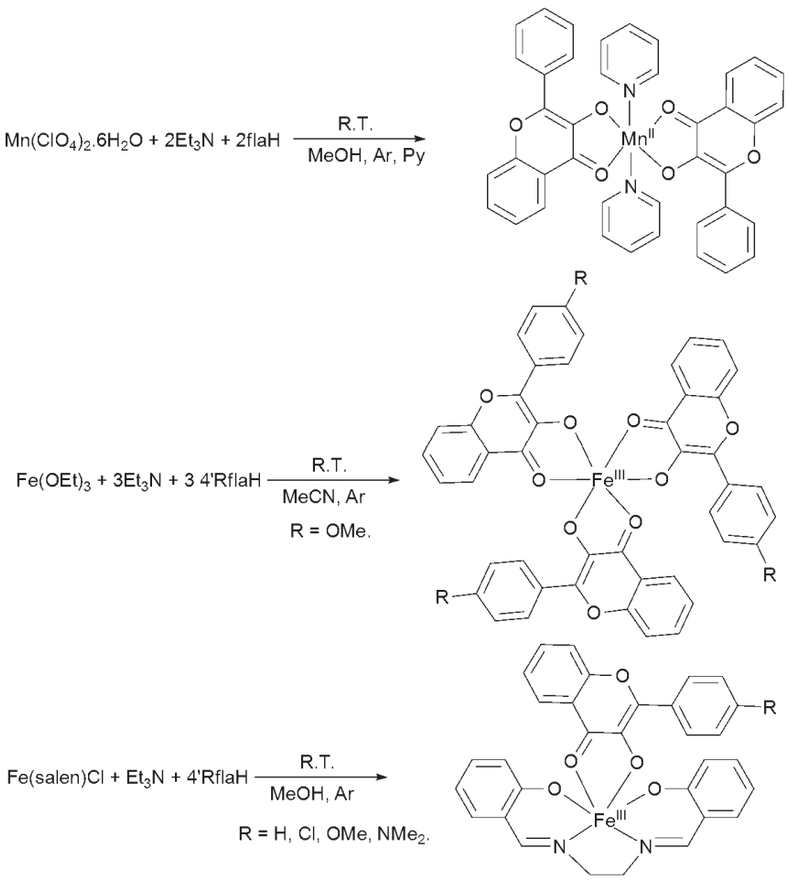


Fig. 3. Formation of manganese(II) and iron(III) flavonolate complexes.

| Complex | | M–O (Å) | $\Delta_{M-O}$ (Å) | IR, $\nu_{CO}$(cm$^{-1}$) | UV-vis, λ (nm) (log $\varepsilon$) |
|---|---|---|---|---|---|
| Cu(fla)$_2$[a] | Cu1–O1<br>Cu1–O2 | 1.942(2)<br>1.900(2) | 0.042 | 1536 | 433 (4.56) |
| Mn(fla)$_2$(py)$_2$[b] | Mn1–O1<br>Mn1–O2 | 2.1839(18)<br>2.1274(16) | 0.057 | 1542 | 433 (4.14) |
| [Mn(6Ph$_2$TPA)(fla)]$^{+}$[c] | Mn1–O1<br>Mn1–O2 | 2.143(3)<br>2.121(3) | 0.022 | 1550 | 431 (4.24) |
| Fe(4′MeOfla)$_3$[b] | Fe1–O1<br>Fe1–O2 | 2.109(8)<br>1.955(7) | 0.154 | 1547 | 411 (4.68) |
| Fe(fla)(salen)[d] | Fe1–O1<br>Fe1–O2 | 2.139(4)<br>1.955(4) | 0.184 | 1549 | 407 (4.25) |
| Fe(4′Clfla)(salen)[d] | | | | 1547 | 411 (4.15) |
| Fe(4′MeOfla)(salen)[d] | | | | 1542 | 445 (4.25) |
| Fe(4′NMe$_2$fla)(salen)[d] | | | | 1536 | 426 (4.56) |

Table 1. Spectroscopic and structural data for synthetic ES type complexes: [a](Pap et al., 2010); [b](Kaizer et al, 2007); [c](Grubel et al., 2010); [d](Baráth et al., 2009).

The manganese-oxygen bond distances are in the range of 2.127–2.184 Å, somewhat longer than those in $Cu^{II}(fla)_2$ (1.901-1944 Å). In the only other Mn(II) flavonolate complex reported to date, [6-$Ph_2$TPA)Mn(fla)]$ClO_4$, the Mn–O distances differ by ~0.06 Å, with the bond involving the ketone oxygen being shorter. The average Mn–O distance in $Mn(fla)_2(py)_2$ (2.13 Å) is longer than that found in [6-$Ph_2$TPA)Mn(fla)]$ClO_4$ (2.16 Å) (Grubel et al., 2010).

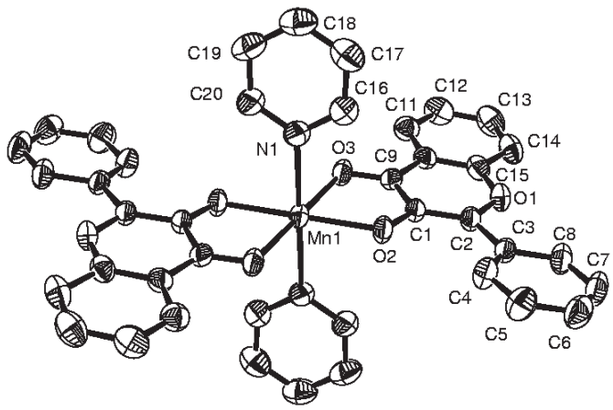


Fig. 4. The molecular structure of $Mn(fla)_2(py)_2$ with selected bond distances (Å) and angles (°) (Kaizer et al, 2007): Mn1–O2 2.1274(16), Mn1–O3 2.1839(18), Mn1–N1 2.348 (2), O1–C15 1.351(3), O1–C2 1.374(3), O2–C1 1.302(3), O3–C9 1.257(3), C1–C9 1.460(3), C1–C2 1.385(3), C10–C15 1.393(3), C9–C10 1.437(4), O2–Mn1–O3 76.81(6), O2–Mn1–N1 90.99(7), N1–Mn1–N1* 180.0.

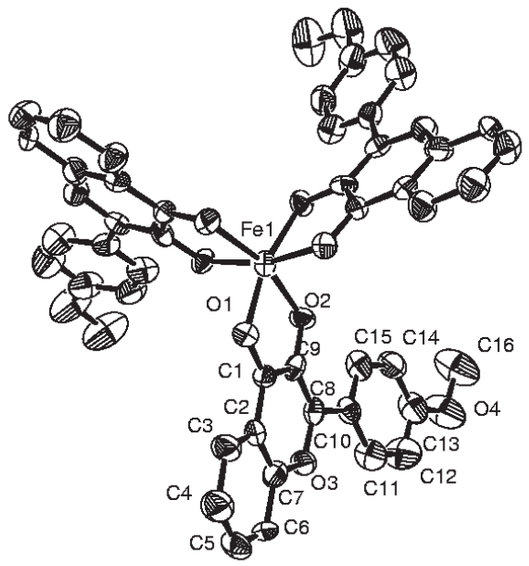


Fig. 5. The molecular structure of $Fe(4'MeOfla)_3$ with selected bond distances (Å) and angles (°) (Kaizer et al, 2007): Fe1–O1 2.109(8), Fe1–O2 1.955(7), O1–C1 1.306(12), O2–C9 1.299(13), O3–C7 1.302(13), O3–C8 1.373(13), C1–C9 1.367(14), C1–C2 1.490(15), C2–C7 1.454(16), C8–C9 1.404(15), O2–Fe1–O1 80.0(3), O1–C1–C9 120.1(9).

The O2–C1 distance is shorter while the O3–C9 distance is longer than those in the uncoordinated flavonol [1.357(3) and 1.232(3) Å]. Due to coordination to the manganese ion there are also changes in the bond lengths of the pyranone ring. The O1–C2 [1.374(3) Å] and C10–C15 [1.393(3) Å] bond lengths become longer, and the C1–C9 bond length [1.460(3) ] is somewhat shorter, which may be assigned to delocalization of the $\pi$-system over the whole molecule (Pap et al., 2010).

The crystal structure of the homoleptic Fe(4'MeOfla)$_3$, shown in Fig. 5 together with selected data, shows a distorted octahedral geometry around the iron(III) center, with all coordination sites being occupied by the bidentate 4'-methoxyflavonolate ligands. The iron-oxygen bond distances are in the range of 1.955–2.109 Å, somewhat longer than those in Cu(fla)$_2$, but somewhat shorter than those in Mn(fla)$_2$(py)$_2$.

The molecular structure and atom numbering scheme for Fe$^{III}$(fla)(salen), shown in Fig. 6 together with selected data, shows a distorted octahedral geometry around the iron(III) center, and that the flavonolate anion is coordinated as a bidentate ligand with a strongly twisted conformation of the salen ligand. The difference in M-O distances ($\Delta_{M\text{-}O}$) are somewhat bigger (0.184 Å) than those in Fe(4'MeOfla)$_3$ (0.154 Å) (Kaizer et al, 2007).

$^{57}$Mösbauer spectrum of the complex exhibits a dominant doublet with isomer shift, $\delta$ = 0.49 mm/s and quadrupole splitting, $\Delta E_Q$ = 1.44 mm/s, indicating a high spin Fe(III) compound (Fig. 7). This is well consistent with the structure of the complex where iron is surrounded by ligands resulting a considerable asymmetric charge distribution reflected by the obtained quadrupole splitting value.

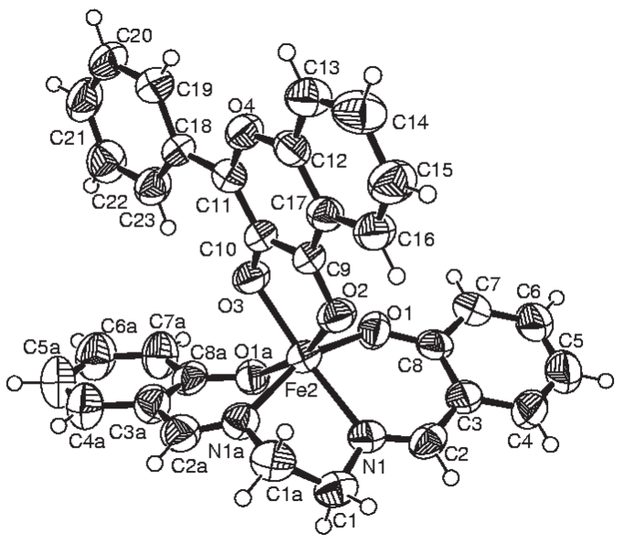


Fig. 6. The molecular structure of Fe(fla)(salen) with selected bond distances (Å) and angles (°) (Baráth et al., 2009): Fe2–O1 1.899(4), Fe2–O1a 1.935(4), Fe2–O3 1.955(4), Fe2–O2 2.139(4), Fe2–N1 2.141(5), Fe2–N1a 2.080(5), O2–C9 1.272(7), O3–C10 1.318(7), C9–C10 1.432(8), C9–C17 1.414(8), C10–C11 1.363(8), C11–O4 1.370(7), C12–O4 1.354(7), N1–C1 1.462(8), N1–C2 1.273(8), N1a–C1a 1.283(8), N1a–C2a 1.283(8), O1a–Fe2–O2 161.72(16), O3–Fe2–N1 158.85(19), O1–Fe2–N1a 158.29(19).

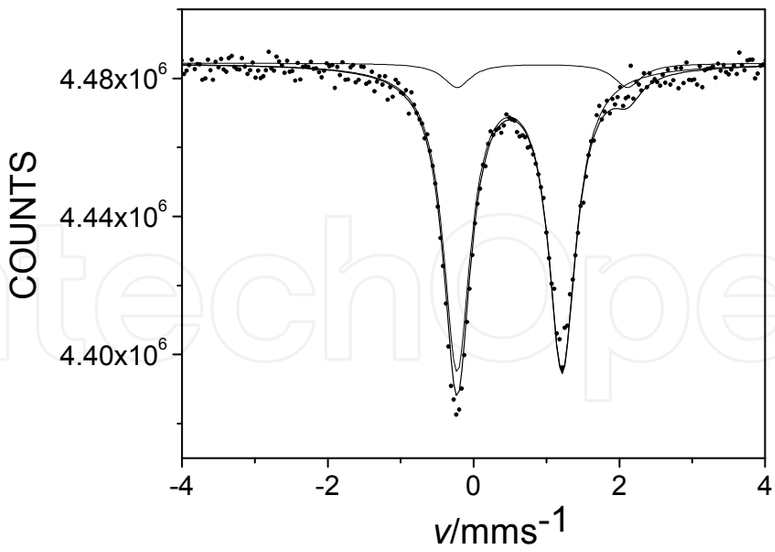


Fig. 7. $^{57}$Fe Mössbauer spectrum, recorded at 80K, of sample Fe(fla)(salen). The dominant doublet with isomer shift, δ=0.49 mm/s and quadrupole splitting, Δ=1.44 mm/s is assigned to high spin Fe(III) in the complex, the minor doublet (δ=0.95 mm/s, Δ=2.34 mm/s, relative area 7 %) represents Fe(II) remaining from the precursor (Baráth et al., 2009).

### 2.2 Synthetic enzyme-product (EP) model

As a synthetic enzyme-product model (*O*-benzoylsalicylato)iron(III) complex (*O*-bsH = *O*-benzoylsalicylic acid) was isolated as a brown solid in ~80% yield by the reaction of Fe(salen)Cl and *O*-benzoylsalicylic acid in the presence of triethylamine at room temperature in methanol. The infrared (IR) spectrum of the complex shows bands corresponding to the coordinated *O*-benzoylsalicylate at 1731 cm$^{-1}$ ($\nu_{CO}$), and 1544, 1385 cm$^{-1}$ ($\nu_{CO2}$).

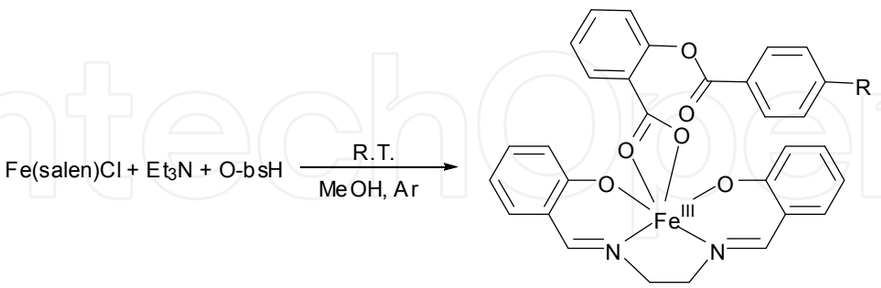


Fig. 8. Formation of iron(III) depside complexes.

The difference between the asymmetric and symmetric stretching frequencies of this carboxylato group [$\Delta\nu = \nu_{as}(CO_2) - \nu_s(CO_2)$] is 159 cm$^{-1}$, rendering these to a bidentate carboxylate bonding mode. The molecular structure of Fe(*O*-bs)(salen) as well as selected bond lengths and angles is shown in Fig. 9. The molecule is monomeric in the solid state. The overall geometry around the six-coordinated iron ion is described as a distorted octahedral geometry.

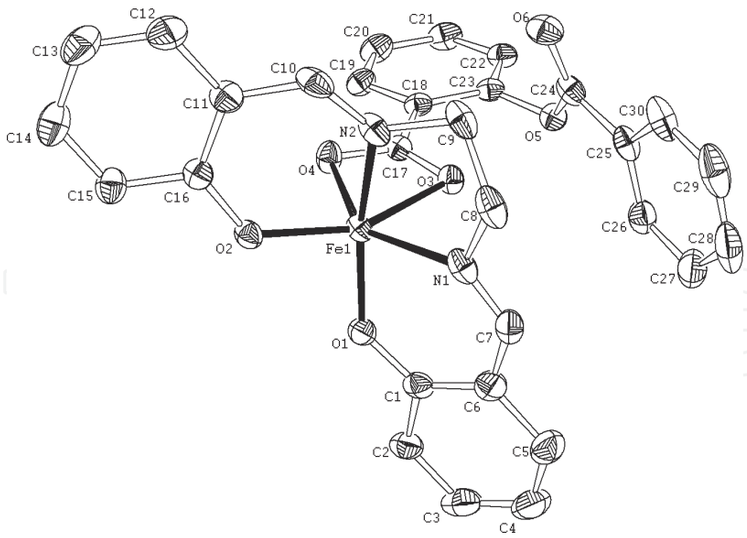


Fig. 9. The molecular structure of Fe(*O*-bs)(salen) with selected bond distances (Å) and angles (°): N1–Fe1 2.131(3), N2–Fe1 2.086(3), N3–Fe2 2.097(3), N4–Fe2 2.117(3), O1–Fe1 1.897(2), O2–Fe1 1.912(2), O3–Fe1 2.156(2), O4–Fe1 2.106(2), O1–Fe1–N2 161.33(12), O4–Fe1–N1 142.59(10), O4–Fe1–O3 61.06(9), O2–Fe1–O3 152.81(10).

### 2.3 Functional models

Flavonolate as a chelating ligand forms stable complexes with copper, manganese and iron ions. Complexes $Mn(fla)_2(py)_2$, $Fe(4'MeOfla)_3$ and Fe(4'Rfla)(salen) are inert to dioxygen in solid form, and even in solution at ambient conditions. At elevated temperature (100-120 °C) the dioxygenation reaction proceeds reasonably fast in DMF. The CO content was determined by GC-MS. The GLC-MS analysis of the residue of the hydrolyzed complexes, after treatment with ethereal diazomethane, showed the presence of the *O*-benzoylsalicylic acid methylester. Oxygenations were also carried out under an atmosphere containing ~60% $^{18}O_2$. Addition of excess of $Et_2O$ into the reaction mixtures resulted in the deposition of the mixture of the corresponding $^{18}O$- and $^{16}O$-benzoylsalicylato manganese and iron complexes [IR (KBr): 1740 ($\nu C^{16}O$) and 1700 $cm^{-1}$ ($\nu C^{18}O$)]. The hydrolyzed acid derivative gave a molecular ion at *m/z* 260 (256+4), showing that both $^{18}O$ atoms of $^{18}O_2$ are incorporated into the carboxylic acid from the molecular oxygen, and the gas phases showed only the presence of unlabeled CO. The relative abundances of *m/z* 260 to that at *m/z* 256 parallel the $^{18}O_2$ enrichments used in the experiments.

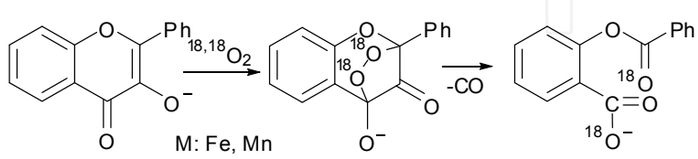


Fig. 10. Reaction of manganese(II) and iron(III) flavonolates with dioxygen (Baráth et al., 2009; Kaizer et al., 2007).

Reactions of $Mn(fla)_2(py)_2$, $Fe(4'MeOfla)_3$ and Fe(fla)(salen) with dioxygen were performed in DMF solutions at 85–120 °C, and the concentration change of the corresponding complex was followed by electronic spectroscopy measuring the absorbance of the reaction mixture

at 433, 411 and 407 nm, respectively. Kinetic studies on the oxygenation of the manganese and iron flavonolate complexes established second-order overall rate expressions – d[M(fla)]/d$t$ = [M(fla)][$O_2$], and all reactions were entropy driven (Table 2), indicating that the rate-determining step is bimolecular (Baráth et al., 2009; Kaizer et al., 2007).

| | $10^2 k^a$/ $M^{-1}s^{-1}$ | $\Delta H^{\#}$/ kJ $mol^{-1}$ | $\Delta S^{\#}$/ J $mol^{-1}$ $K^{-1}$ | $\rho$ |
|---|---|---|---|---|
| Fe(4'MeOfla)$_3$ | 50 | 40 | -144 | - |
| Fe(fla)(salen) | 2.07 | 76 | -94 | -0.54 |
| Fe(4'Clfla)(salen) | 1.26 | - | - | - |
| Fe(4'MeOfla)(salen) | 2.90 | - | - | - |
| Fe(4'NMe$_2$fla)(salen) | 5.07 | - | - | - |
| Mn(fla)$_2$(py)$_2$ | 8 | 49 | -137 | - |
| Cu(fla)$_2$ | 0.87 | 53 | -138 | -0.63 |

Table 2. Kinetic data for the oxygenation of metal flavonolates (Baráth et al., 2009; Kaizer et al., 2007; Pap et al., 2010).

The influence of the 4'-substituted groups on the reaction rate of Fe(4'Rfla)(salen) and Cu(4'Rfla)$_2$ complexes showed a linear Hammett plot with a reaction constant of $\rho$=-0.54 and -0.63, respectively, indicating that the electron-releasing groups result in reamarkable increase in the reaction rates. On the basis of the kinetic data (compared to our earlier copper-containing systems), it can be said that there is no significant effect of the metal used in our model experiments, suggesting a same mechanism (Pap et al., 2010; Kaizer et al., 2006).
Beside the electronic factors the steric effect was also investigated on the dioxygenation reaction of Fe(fla)(salen). We have found that the rate of dioxygenolysis is dramatically enhanced by various coligands, such as acetate ($CH_3CO_2^-$), phenyl- ($PhCH_2CO_2^-$), diphenyl- ($Ph_2CHCO_2^-$) or triphenylacetate ($Ph_3CCO_2^-$) (Fig. 11).

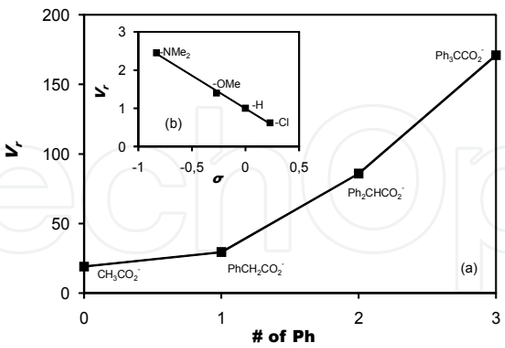


Fig. 11. (a) Steric effects on the reaction rate for the dioxygenation of Fe(fla)(salen) in the presence of 10 equiv acetates in DMF at 100 °C (correlation between the number of phenyl substituents of acetates and the relative rates) (b) Substituent effects on the rate constants for the dioxygenation of Fe(fla)(salen) in DMF at 100 °C (Baráth et al., 2009).

For example, addition of 10 equivalents of the bulky $Ph_3CCO_2^-$ to Fe(fla)(salen) accelerated its decay by two order of magnitude ($V_r$ = 171) at 100 °C, and the reaction above can take place even at ambient temperature (20 °C). The kinetics of the carboxylate-enhanced

dioxygenation of $Fe^{III}$(fla)(salen) measured at 40 °C (Fig. 12) resulted in a rate equation with first order dependence on Fe(fla)(salen), dioxygen and triphenylacetate ($k$ = (5.02 ± 0.35) × $10^2$ $M^{-2}$ $s^{-1}$, $\Delta H^{\#}$ = 35 kJ $mol^{-1}$, $\Delta S^{\#}$ = -120 J $mol^{-1}$ $K^{-1}$ at 313.16 K).

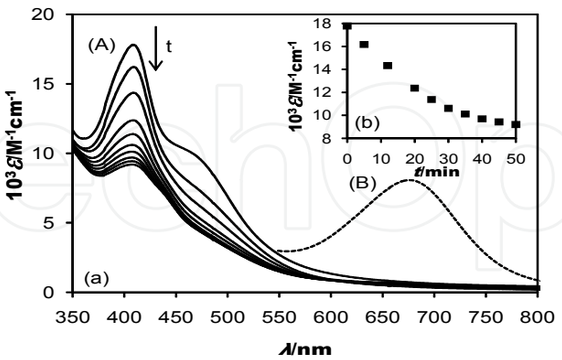


Fig. 12. (a) (A) Visible spectral change for the decay of Fe(salen)(fla) in the presence of 10 eq. $Ph_3CCO_2^-$ in DMF at 40 °C, (B) in the presence of NBT. (b) Time-dependent conversion of Fe(fla)(salen) under the condition described above monitored at 407 nm (Baráth et al., 2009).

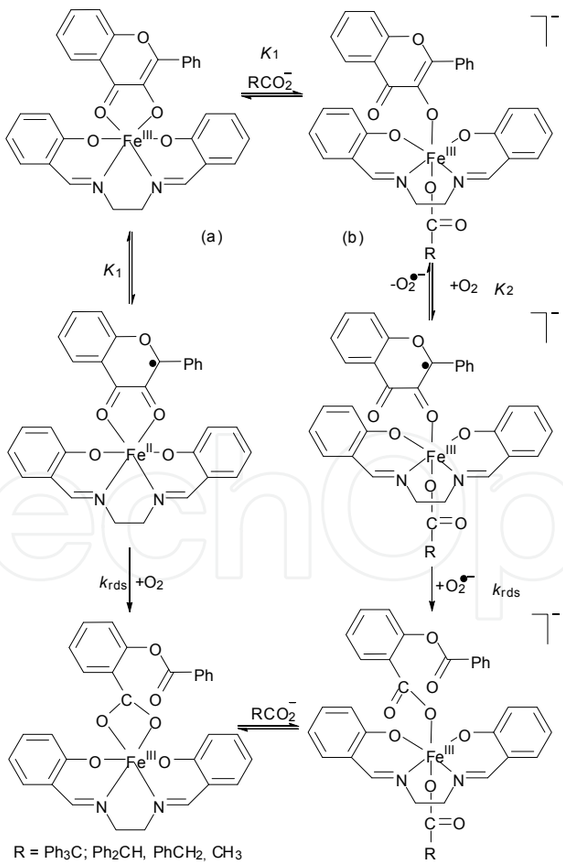


Fig. 13. Mechanistic differences between the direct and carboxylate-enhanced oxygenation of Fe(fla)(salen) (Baráth et al., 2009).

The main mechanistic difference between the direct and carboxylate-enhanced dioxygenation of Fe(fla)(salen) is that in the latter case there is an electron transfer from Fe(fla)(salen) to dioxygen resulting in the formation of free superoxide radical anion which was proved by the test for free superoxide radical anion with nitroblue tatrazolium (NBT), where the reduction of the added dye to the blue diformazan took place (Fig. 12). Same behavior was found for the enzyme-like oxygenation of [Cu(fla)(idpa)]$ClO_4$ in the presence and absence of carboxylate co-ligands (Pap et al., 2010). On the basis of chemical, spectroscopic and kinetic data it can be said that bulky carboxylates as coligands dramatically enhance the reaction rate, which can be explained by two different pathways, caused by the formation of more reactive monodentate flavonolatoiron complexes (Fig. 13). An analogous reaction pathway, direct electron transfer from the activated flavonol to dioxygen without the need for redox cycling of the metal (b), was suggested for our earlier potassium and zinc-containing model systems, and the Ni- and Co-containing flavonol 2,4-dioxygenase (Merkens et al., 2008).

## 3. Conclusion

As a conclusion it can be said that in the enzyme-like oxygenation of the coordinated flavonolate ligand by manganese(II) or iron(III), the formation of endoperoxide in bimolecular reactions can be assumed, and their decomposition by loss of carbon monoxide results in the corresponding depside as a good mimic of the enzyme action. Furthermore it was shown that bulky carboxylates as coligands dramatically enhance the reaction rate, which can be explained by two different mechanisms, caused by the formation of more reactive monodentate iron(III) flavonolate complexes.

## 4. Acknowledgments

The authors are grateful for the financial support of the grant TAMOP-4.2.1/B-09/1/KONV-2010-0003: Mobility and Environment: Researches in the fields of motor vehicle industry, energetics and environment in the Middle- and West-Transdanubian Regions of Hungary. The Project is supported by the European Union and co-financed by the European Regional Development Fund. Financial support of the Hungarian National research Fund (OTKA K67871 and K75783) is also gratefully acknowledged.

## 5. References

Baráth, G. ; Kaizer, J. ; Speier, G. ; Párkányi, L. ; Kuzmann, E. & Vértes, A. (2009). One metal – two pathways to the carboxylate-enhanced, iron-containing quercetinase mimics. *Chemical Communications*, Issue 24, pp. 3630-3632, ISSN 1359-7345.

Barhács, L. ; Kaizer, J. & Speier, G. (2000). Kinetics and mechanism of the oxygenation of potassium flavonolate. Evidence for an electron transfer mechanism. *Journal of Organic Chemistry*, Vol.65, Issue 11, (Jun 2000), pp. 3449-3452, ISSN 0022-3263.

Barney, B. M. ; Schaab, M. R.; LoBrutto, R. & Francisco, W. A. (2004). Evidence for a new metal in a known active site : Purification and characterization of an iron-containing quercetin 2,3-dioxygenase from *Bacillus subtilis*. *Protein Expression & Purification*, Vol.35, No.1, (May 2004), pp. 131-141, ISSN 1046-5928.

Bowater, L. ; Fairhurst, S. A. ; Just, V. J. & Bornemann, S. (2004). *Bacillus subtilis* YxaG is a novel Fe-containing quercetin 2,3-dioxygenase, *FEBS Letters*, Vol.557, Issue 1-3, (January 2004), pp. 45-48, ISSN 0014-5793.

Bugg, T. D. H. (2001). Oxygenases : Mechanisms and structural motifs for $O_2$ activation. *Current Opinion in Chemical Biology*, Vol.5, Issue 5, (October 2001), pp. 550-555, ISSN 1367-5931.

Bugg, T. D. H. & Ramaswamy, S. (2008). Non-heme iron-dependent dioxygenases : unravelling catalytic mechanisms for complex enzymatic oxidations. *Current Opinion in Chemical Biology*, Vol.12, Issue 2, (April 2008), pp. 134-140, ISSN 1367-5931.

Fusetti, F. ; Schröter, K. H. ; Steiner, R. A. ; van Noort, P. I. ; Pijning, T. ; Rozeboom, H. J. ; Kalk, K. H. ; Egmond, M. R. & Dijkstra, B. W. (2002). Crystal structure of the copper-containing quercetin 2,3-dioxygenase from *Aspergillus japonicus*. *Structure*, Vol.10, Issue 2, (February 2002), pp. 259-268, ISSN 0969-2126.

Gopal, B. ; Madan, L. L. ; Betz, S. F. & Kossiakoff, A. A. (2005). The crystal structure of a querceti 2,3-dioxygenase from *Bacillus subtilis* suggests modulation of enzyme activity by a change in the metal ion at the active site(s). *Biochemistry*, Vol.44, Issue 1, (January 2005) pp. 193-201, ISSN 0006-2960.

Grubel, K. ; Rudzka, K. ; Arif, A. M. ; Halfen, J. A. & Berreau, L. M. (2010). Synthesis, characterization, and ligand exchange reactivity of a series of first row divalent metal 3-hydroxyflavonolate complexes. *Inorganic Chemistry*, Vol.49, No.1, (January 2010), pp. 82-96, ISSN 0020-1669.

Hund, H. K. ; Breuer, J. ; Lingens, F. ; Hüttermann, J. ; Kappl. R. & Fetzner, S. (1999). Flavonol 2,4-dioxygenase from *Aspergillus niger* DSM 821, a type 2 Cu-II-containing glycoprotein. *Europian Journal of Biochemistry*, Vol.263, Issue 3, (August 1999) pp. 871-878, ISSN 1742-4658.

Kaizer, J. ; Balogh-Hergovich, É. ; Czaun, M. ; Csay, T. & Speier, G. (2006). Redox and nonredox metal assisted model systems with relevance to flavonol and 3-hydroxyquinolin-4(1H)-one 2,4-dioxygenase. *Coordination Chemistry Reviews*, Vol.250, Issue 17-18, (September 2006), pp. 2222-2233, ISSN 0010-8545.

Kaizer, J. ; Baráth, G. ; Pap, J. ; Speier, G. ; Giorgi, M. & Réglier, M. (2007). Manganese and iron flavonolates as flavonol 2,4-dioxygenase mimics. *Chemical Communications*, Issue 48, (pp. 5235-5237), ISSN 1359-7345.

Kovaleva, E. G. & Lipscomb, J. D. (2007). Crystal structures of $Fe^{2+}$ dioxygenase superoxo, alkylperoxo, and bound product intermediates. *Science*, Vol.316, No.5823, (April 2007), pp. 453-457, ISSN 1095-9203.

Kooter, I. M. ; Steiner, R. A. ; Dijkstra, B. W. ; van Noort, P. I. ; Egmond, M. R. & Huber, M. (2002). EPR characterization of the mononuclear Cu-containing *Aspergillus japonicus* quercetin 2,3-dioxygenase reveals dramatic changes upon anaerobic binding of substrates. *Europian Journal of Biochemistry*, Vol.269, Issue 12, (June 2002), pp. 2971-2979, ISSN 1742-4658.

Merkens, H. ; Sielker, S. ; Rose K. & Fetzner, S. (2007). A new monocupin quercetinase of Streptomyces sp. FLA : Identification and heterologous expression of the *queD* gene and activity of the recombinant enzyme towards different flavonols. *Archives of Microbiology*, Vol. 187, Issue 6, (June 2007), pp. 475-487, ISSN 0302-8933.

Merkens, H. ; Kappl, R. ; Jakob, R. P. ; Schmid, F. X. & Fetzner, S. (2008). Quercetinase QueD of *Streptomyces sp*. FLA, a monocupin dioxygenase with a preference for nickel and cobalt. *Biochemistry*, Vol.47, Issue 46, (November 2008) pp. 12185-12196, ISSN 0006-2960.

Oka, T. ; Simpson, F. J. & Krishnamurty, H. G. (1972). Degradation of rutin by Aspergillus flavus : Studies on specificity, inhibition, and possible reaction mechanism of quercetinase. *Canadian Journal of Microbiology*, Vol.18, Issue 4, (April 1972), pp. 493-508, ISSN 1480-3275.

Pap, J. S. ; Kaizer, J. & Speier, G. (2010). Model systems for the CO-releasing flavonol 2,4-dioxygenase enzyme. *Coordination Chemistry Reviews*, Vol.254, Issue 7-8, (April 2010), pp. 781-793, ISSN 0010-8545.

Schaab, M. R. ; Barney, B. M. & Francisco, W. A. (2006). Kinetic and spectroscopic studies on the quercetin 2,3-dioxygenase from *Bacillus subtilis*. *Biochemistry*, Vol.45, Issue 3, (January 2006), pp. 1009-1016, ISSN 0006-2960.

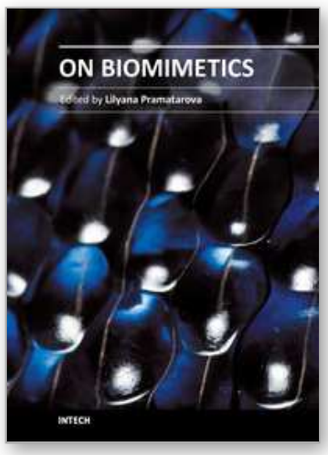


**On Biomimetics**

Edited by Dr. Lilyana Pramatarova

ISBN 978-953-307-271-5
Hard cover, 642 pages
**Publisher** InTech
**Published online** 29, August, 2011
**Published in print edition** August, 2011

Bio-mimicry is fundamental idea â€˜How to mimic the Natureâ€™ by various methodologies as well as new ideas or suggestions on the creation of novel materials and functions. This book comprises seven sections on various perspectives of bio-mimicry in our life; Section 1 gives an overview of modeling of biomimetic materials; Section 2 presents a processing and design of biomaterials; Section 3 presents various aspects of design and application of biomimetic polymers and composites are discussed; Section 4 presents a general characterization of biomaterials; Section 5 proposes new examples for biomimetic systems; Section 6 summarizes chapters, concerning cells behavior through mimicry; Section 7 presents various applications of biomimetic materials are presented. Aimed at physicists, chemists and biologists interested in biomineralization, biochemistry, kinetics, solution chemistry. This book is also relevant to engineers and doctors interested in research and construction of biomimetic systems.

**How to reference**

In order to correctly reference this scholarly work, feel free to copy and paste the following:

József Kaizer, József Sándor Pap and Gábor Speier (2011). Iron and Manganese-Containing Flavonol 2,4-Dioxygenase Mimics, On Biomimetics, Dr. Lilyana Pramatarova (Ed.), ISBN: 978-953-307-271-5, InTech, Available from: http://www.intechopen.com/books/on-biomimetics/iron-and-manganese-containing-flavonol-2-4-dioxygenase-mimics

INTECH
open science | open minds

**InTech Europe**
University Campus STeP Ri
Slavka Krautzeka 83/A
51000 Rijeka, Croatia
Phone: +385 (51) 770 447
Fax: +385 (51) 686 166
www.intechopen.com

**InTech China**
Unit 405, Office Block, Hotel Equatorial Shanghai
No.65, Yan An Road (West), Shanghai, 200040, China
中国上海市延安西路65号上海国际贵都大饭店办公楼405单元
Phone: +86-21-62489820
Fax: +86-21-62489821

IntechOpen